THE ASTROPHYSICAL JOURNAL, 453:754–760, 1995 November 10

THE INFRARED NEBULA AND OUTFLOW IN LYNDS 483

G. A. FULLER[1,2]
National Radio Astronomy Observatory,[3] Edgemont Road, Charlottesville, VA 22903
E. A. LADA[2,4]
Astronomy Department, University of Maryland, College Park, MD 20742
AND
C. R. MASSON AND P. C. MYERS[2]
Harvard-Smithsonian Center for Astrophysics, 60 Garden Street, Cambridge, MA 02138
Received 1994 December 14; accepted 1995 May 18

ABSTRACT

Near-infrared and submillimeter observations of IRAS 18148−0440 in the Lynds 483 dark cloud are presented. The near-infrared images show nebulous emission extending up to ∼60″ from the *IRAS* position. The *IRAS* source is not directly detected at any wavelength and is obscured by more than 70 mag of visual extinction. Submillimeter continuum measurements indicate the presence of $\sim 0.3\ M_\odot$ of material within about 1900 AU of the central star. At 2.2 μm the near-infrared nebula is bipolar with approximately cylindrical lobes which extend east and west of the *IRAS* source and coincide with the bipolar lobes of the CO outflow from the source. The western lobe of the nebula is significantly brighter than the eastern lobe and is spatially coincident with the blueshifted CO emission from the outflow. If the nebular lobes have equal intrinsic brightness, their apparent brightness implies that the outflow has an inclination angle of ∼40° to the plane of the sky and that the density distribution within the dense gas around IRAS 18148−0440 has a radial profile steeper than r^{-1}. There is a bright knot of molecular hydrogen emission close to the end of the blueshifted CO with a jet like feature extending from the knot back toward the location of the embedded star. The knot of emission is thought to be tracing the region where the stellar wind is impacting the surrounding dense gas. The observations suggest that IRAS 18148−0440 is very young and that its outflow is driven by a jet from the central star.

Subject headings: infrared: ISM: continuum — ISM: individual (L483) — ISM: jets and outflows — ISM: structure — radio lines: ISM

1. INTRODUCTION

Near-infrared observations can provide important information on at least two aspects of the circumstellar environment of young stars. First, near-infrared images show that many young stars are associated with regions of extended emission (e.g., Kenyon et al. 1993b; Tamura et al. 1991). In many cases this extended emission is radiation from the young star which is scattered by dense material near the star. These near-infrared nebulae can therefore provide a relatively high angular resolution view of the circumstellar material associated with the stars. In addition, the many transitions of molecular hydrogen which lie in the near-infrared windows can be used to study the interaction between the outflow from a star and the dense material around the star (e.g., Bally, Lada, & Lane 1993).

Some young stars, such as the well-known object L1551 IRS 5 (Hodapp et al. 1988), have such large extinctions along the direct line of sight to the star that only scattered radiation is detectable. The large extinctions to such stars suggest that they are very young, with ages of less than 10^5 yr. The rapid evolutionary timescale for these young stars assures that there are relatively few of these objects and therefore each new such object found can provide important information on the process of star formation.

In this paper we present recent near-infrared and submillimeter continuum and CO observations of the very young star, IRAS 18148−0440 in the opacity class 6 Lynds dark cloud 483. Parker (1988, 1991) first identified this source as associated with the dark cloud and suggested its protostellar nature and young age based on its *IRAS* colors. The source has an *IRAS* luminosity of 9 $L_\odot$, assuming a distance of 200 pc. Parker, Padman, & Scott (1991) have identified a bipolar outflow from the source, and strong outflow activity is also suggested by the presence of water maser emission (Wilking et al. 1994). Observations of NH_3 and HC_3N show the *IRAS* source to be very well centered in a region of dense gas (Fuller & Myers 1993). A 3.6 cm continuum source coincident with the *IRAS* source has recently been detected by Anglada et al. (1995).

2. OBSERVATIONS AND DATA REDUCTION

In 1993 July, IRAS 18148−0440 was observed with the KPNO 2.1 m telescope using the KPNO infrared imager (IRIM) containing a 256 × 256 NICMOS III chip. The instrument was configured with 1.″09 pixels giving a field of view of 279″ on a side. Observations were made using *J*, *H*, and *K*′ broadband filters and narrowband filters centered at 2.12 μm with a 0.021 μm bandpass and at 2.22 μm with a 0.089 μm bandpass. These narrowband filters are centered on the $v = 1$–$0\ S(1)$ line of H_2 and a nearby region of line free continuum, respectively.

The broadband images were flux-calibrated using observations of standard stars, assuming the stars had the same *K*

[1] Jansky Fellow.
[2] Visiting Astronomer, Kitt Peak National Observatory.
[3] Operated by Associated Universities, Inc., under cooperative agreement with the National Science Foundation.
[4] Hubble Fellow.

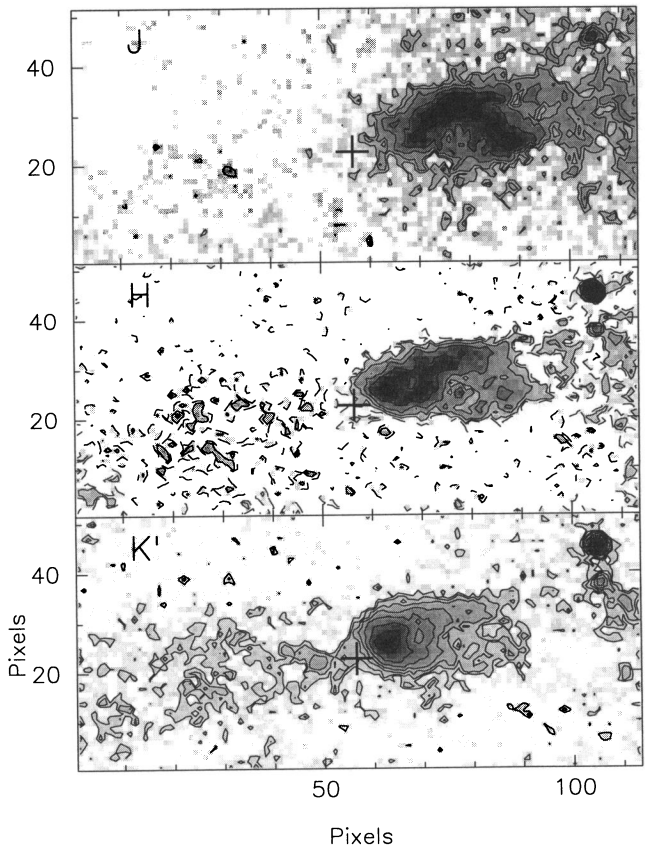

FIG. 1.—*J*, *H*, and *K'* (*top to bottom*) images toward IRAS 18148−0440. The axes are marked in pixels from the lower left corner of the image. Each pixel is 1.″09 on a side. The cross in each panel marks the approximate location of the *IRAS* source and the VLA continuum source (R.A.[1950] = $18^h14^m50^s.62$, decl.[1950] = −04°40′49″.4). The contour levels start at 21.9, 20.9, and 19.3 mag arcsec^{-2} for the *J*, *H*, and *K'* images, respectively. The contour interval is 0.5 mag arcsec^{-2} for all the images. North is up and east is to the left.

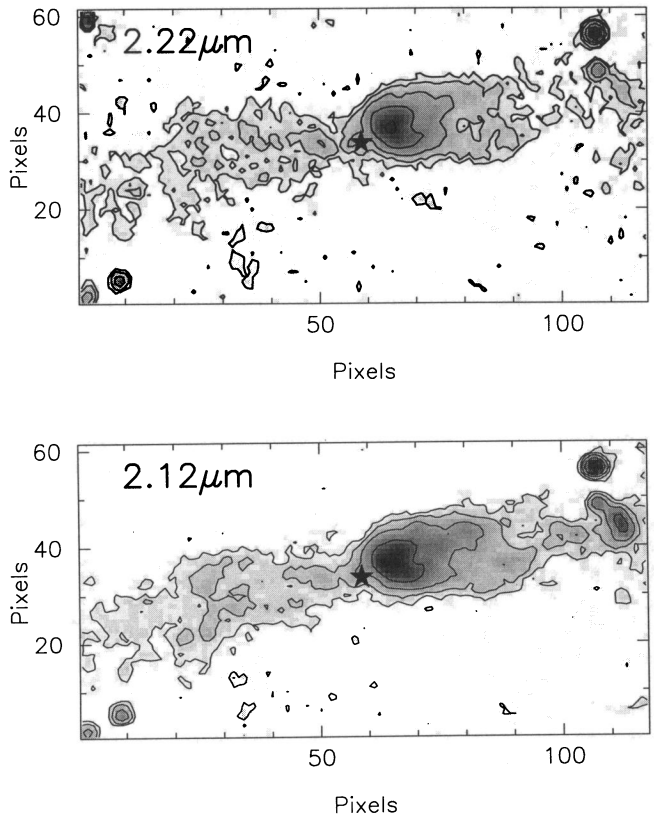

FIG. 2.—Images toward IRAS 18148−0440 at 2.22 μm (*upper*) and 2.12 μm (*lower*). The contour levels for both images start at 20 mag arcsec^{-2} and increase in steps of 1 mag arcsec^{-2}. North is up, and east to the left. The knot of emission at the western end of the western lobe and its connection back to the peak of the nebula are much more apparent in the 2.12 μm image. Each pixel is 1.″09 on a side.

and *K'* magnitudes. When forming the image of the molecular hydrogen emission, the 2.12 μm and 2.22 μm images were convolved to the same point spread function (psf) by convolving each with the other's psf. The 2.22 μm image was then scaled to obtain the best possible cancellation of the stellar images under the assumption that the stars should have no spectral features from molecular hydrogen. The weather during the observations was variable. Comparison of different observations of standard stars and earlier observations of the nebula at *K*, we estimate an uncertainty in the calibration (including the assumed *K'* magnitudes of the standards) of ∼15%.

IRAS 18148−0440 is in a region of high visual extinction and even on the largest mosaic obtained, there are no visible stars with known positions. The position of the near-infrared nebula is therefore uncertain. However, it is clear that the peak of the *K'* nebula is offset from the position of the *IRAS* source and radio continuum source by 7″–10″. Measurements made by offsetting the telescope from a nearby SAO star in 1993 July, and during earlier observing sessions in 1991 and 1992, indicate that the peak of the nebula at *K'* is ∼10″ west of the *IRAS* (and radio continuum) position. Measurements of the position on the chip of a photometric standard star before an observation of the nebula at *K'* located the *IRAS* source about 3″ closer to the peak of the *K'* nebula. This is the location marked on Figures 1 and 2.

IRAS 18148−0440 was observed at 1100 μm, 800 μm, and 450 μm with the James Clerk Maxwell Telescope (JCMT)[5] in Hawaii on 1993 March 1. The weather was very stable during the observations with a zenith optical depth at 225 GHz between 0.04 and 0.05. The observing method and data reduction are described in more detail in Jensen, Mathieu, & Fuller (1995). The beam size for these measurements was 19″. The measured fluxes of IRAS 18148−0440 and the statistical uncertainties are 0.64 ± 0.02 Jy at 1100 μm, 1.98 ± 0.02 at 800 μm, and 15 ± 2 Jy at 450 μm.

Observations of CO $J = 3 \rightarrow 2$ were obtained toward IRAS 18148−0440 on 1992 May 28 using the Caltech Submillimeter Observatory[6] (CSO). Several "on-the-fly" maps of the CO emission were made by collecting data while raster scanning the telescope across the source. The data were binned to a 10″ grid which corresponds to one-half the beam FWHM at the frequency of the CO line. The final map presented here was

[5] The James Clerk Maxwell Telescope is operated by the Royal Observatories on behalf of the Particle Physics and Astronomy Research Council of the United Kingdom, the Netherlands Organization for Scientific Research, and the National Research Council of Canada.

[6] The CSO is operated by the California Institute of Technology under funding from the National Science Foundation, contract AST 90-15755.

constructed by averaging two on-the-fly maps. Before averaging, these maps were compared and found to be consistent in their line amplitudes and in the location of the CO emission.

3. RESULTS

The J, H, and K' broadband images of the region around IRAS 18148−0440 in L483 are shown in Figure 1. Each image shows the same region and the images have been aligned assuming that the star at the northwestern corner of the frame has the same position at all wavelengths.

There is significant near-infrared emission in all three broadband filters which extends up to 1′ from the *IRAS* location. At K', the emission has a total extent of ∼2′. The bulk of the emission at all the wavelengths is to the west of the *IRAS* source. However, both the location and shape of the emission region change with wavelength. At the shortest wavelength, J, the emission arises from an arc-shaped region which peaks about ∼8″ north and ∼24″ west of the *IRAS* position. At lower levels the emission extends farther westward. At H, the peak of the emission is closer to the *IRAS* source position. At this wavelength there are two stars detected in the northwestern corner of the region shown in the figure. Both stars are also clearly detected at K' and the brighter, northern star is also detected at J.

At K', the emission arises primarily from a region similar in shape and location to the H nebula. There are two other important features which are apparent in the K' image: the low-level emission to the east of the *IRAS* source and the apparently isolated knot of emission about 55″ west and 11″ north of the *IRAS* source. There is some hint of both these features in the H image but they are both much more apparent in the K' image.

Figure 2 shows deeper 2.12 μm and 2.22 μm narrow band images of IRAS 18148−0440. Overall, the nebular emission in these two images is similar in shape and extent to that in the K' image; however, in both images the eastern lobe of the nebula is much better detected than at K'. As can be seen from the figure, the eastern lobe has a smoother brightness distribution than the western lobe of the nebula. One notable feature of both the eastern and western lobes of the nebula is that they have approximately constant size perpendicular to their long axis, except in the immediate vicinity of the *IRAS* source. This cylindrical shape is in marked contrast to many K-band nebulae around young stars where the outer edge of the nebula appears parabolic or conical in shape (for example, Hodapp et al. 1988; Aspin et al. 1991; Tamura & Yamashita 1992).

At 2.12 μm the knot of emission at the western end of the western lobe of the nebula is much brighter than in either the K' or 2.22 μm images and is connected by a region of lower level emission to the peak of the nebula. At 2.22 μm, any connection between the knot of emission and the peak of the nebula is significantly weaker. The enhanced brightness of the western knot of emission at 2.12 μm, and the region between it and the peak of the nebula, relative to the line-free 2.22 μm filter, is indicative of $v = 1$–0 $S(1)$ molecular hydrogen emission. These differences in the morphology of the nebula indicate the presence of molecular hydrogen, independent of the relative calibration of the two narrowband images.

The image of the H_2 emission formed from the difference of the 2.12 μm and the 2.22 μm images (§ 2) is shown in Figure 3. The bright knot ∼55″ west of the IRAS 18148−0440 source which is apparent in the 2.12 μm image is clearly the strongest source of H_2 emission. The emission connecting this bright knot to the peak of the nebula in the 2.12 μm image is visible in the molecular hydrogen emission as a jetlike feature extending from the bright knot back toward the location of the *IRAS* source. This jet terminates near a second fainter, but more extended, region of H_2 emission close to the location of the peak of the K' nebula.

The CO $J = 3 \rightarrow 2$ emission, integrated over the velocity ranges −2 to 4 km s^{-1} and 6–14 km s^{-1}, is also shown in Figure 3. The CO arises from two spatially separated lobes of emission. The redshifted emission peaks about 30″ east (and 10″ south) of the *IRAS* source and is extended almost due east. The blueshifted emission peaks 20″ west of the *IRAS* source, and extends from close to the *IRAS* source due west about 70″. The overall shape of the CO lobes is very similar to that of the 2 μm nebula. The CO $J = 3 \rightarrow 2$ emission is almost identical in shape, extent, and the location of the peaks to the CO $J = 2 \rightarrow 1$ emission from the outflow mapped with the same angular resolution by Parker et al. (1991). The total extent of the CO outflow lobes is ∼170″ (at brightness levels below those shown in Fig. 3). However, the lobes of the CO emission are only 30″–40″ wide. After correcting for the 20″ beamwidth

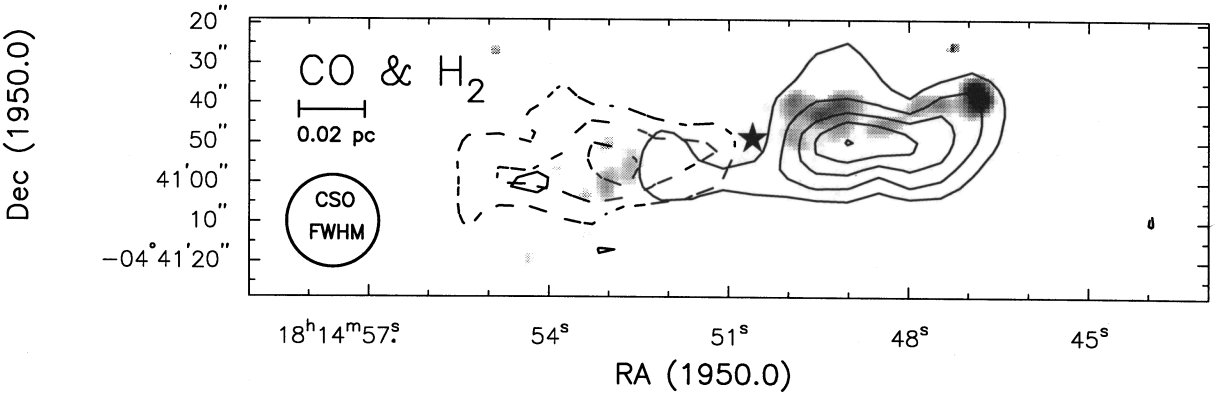

FIG. 3.—The H_2 emission and CO $J = 3 \rightarrow 2$ outflow emission from IRAS 18148−0440. The dashed contours show the redshifted emission integrated over the range from 6 to 14 km s^{-1}. The solid contours show the blueshifted emission integrated from −2 to 4 km s^{-1}. Contour levels for each lobe start at 10 K km s^{-1} and increase in steps of 5 K km s^{-1}. The grayscale shows the molecular hydrogen emission determined from the difference of the narrowband images shown above. The bright knot of H_2 emission is located at the end of the blueshifted CO lobe. Due to uncertainties in the absolute positions of both the CO map and the near-infrared image, the alignment of the images is uncertain by up to 8″. A scale bar and the FWHM of the CSO beam used to make the CO observations are shown to the left.

of the CSO, this implies an aspect ratio for the outflow of 5:1 or greater. The brighter emission shown in Figure 3 is barely resolved across the outflow axis, suggesting that there is significant unresolved small-scale structure in the outflow.

The total integrated emission in the CO $J = 3 \rightarrow 2$ line, including the line core emission, is very similar in shape and extent to the sum of the red and blueshifted emission shown in Figure 3. Little CO $J = 3 \rightarrow 2$ emission is detected north and south of the *IRAS* source even though NH_3 and HC_3N observations show the presence of dense gas at these locations (Fuller & Myers 1993). The weakness of the CO emission from this material relative to the outflowing material suggests that the outflow is warmer than the surrounding dense core gas.

After correcting the observed size of the CO lobes for the 40° inclination angle of the outflow (§ 4.2), each lobe of the CO outflow has a linear extent of $\sim 22 \times 10^3$ AU. Adopting an outflow velocity of 5 km s^{-1} from the CO and correcting for the inclination angle gives a dynamical age of $\sim 13 \times 10^3$ yr.

Comparing the CO and H_2 emission shows that the jetlike feature is projected onto the blueshifted CO emission. The bright knot of molecular hydrogen emission at the western end of the jet is located at the westernmost tip of the blueshifted CO emission. The association of the knot with the CO outflow suggests that this molecular hydrogen emission is tracing the cooling region associated with a shock driven into the gas surrounding IRAS 18148−0440 by its outflow.

The H_2 emission knot at the end of the blueshifted CO lobe has a measured luminosity of 6×10^{-5} $L_\odot$ in the $v = 1$–0 $S(1)$ line (neglecting any foreground extinction). This corresponds to a total molecular hydrogen luminosity for the knot of 6×10^{-4} $L_\odot$, assuming that 10% of the H_2 luminosity is emitted in the $v = 1$–0 $S(1)$ line, as is predicted for 2500 K gas (Scoville et al. 1982). Adopting an outflow luminosity of 5×10^{-3} $L_\odot$ corresponding to the midpoint of the luminosity range of the IRAS 18148−0440 outflow found by Parker et al. (1991), this single H_2 emission knot radiates about 10% of the outflow mechanical luminosity. When corrected for the higher foreground extinction, the fainter but extended H_2 emission closer the star probably has a luminosity comparable to that of the bright knot.

4. DISCUSSION

At near-infrared wavelengths the emission from IRAS 18148−0440 is dominated by extended emission which extends at least 60″ from the location of the *IRAS* source associated with the embedded young star. However, at J and H, no emission is detected at the location of the IRAS 18148−0440 source. The noise levels and psf in these images indicate upper limits on the point source brightness of 18.8 and 18.2 mag at J and H, respectively. At K', there is some emission detected at the location of the *IRAS* source but this is part of the extended nebular emission and shows no pointlike component. We estimate an upper limit of ~ 16.8 mag at K' for the pointlike component at the location of the *IRAS* source.

A lower limit estimate of the brightness of the source illuminating the nebula can be obtained from the surface brightness of the nebula and its angular extent, assuming that the observed nebula is all scattered radiation and that the dust has an albedo of 1 (Hubble 1922). From Figure 1, the western lobe of the nebula has a surface brightness of 21.4 mag $arcsec^{-2}$ at 60″ from the *IRAS* source at J, 20.4 mag $arcsec^{-2}$ at 48″ at H, and 19.3 mag $arcsec^{-2}$ at 37″ at K'. These values imply the brightness of the illuminating source is 9.7, 9.2, and 8.7 magnitudes at J, H, and K', respectively. Comparing these values with the upper limits on the brightness of the central source directly toward the *IRAS* source, the measurement at K' indicate that the line of sight to the *IRAS* source has greater than 70 mag more visual extinction than the path along which the nebula is illuminated. The *IRAS* source therefore has a considerable amount of circumstellar material. Any extinction in front of the nebula which has been ignored in this estimate would increase the estimated amount of extinction directly toward the *IRAS* source.

4.1. *The Spectral Energy Distribution of* IRAS 18148−0440

Figure 4 shows the spectral energy distribution (SED) of IRAS 18148−0440 including the J and H upper limits and the submillimeter measurements from JCMT. The K' limit is not shown as it is more uncertain than the J and H limits because of the nebular emission at the position of the central young star (§ 4). The measurements from 12 μm to 190 μm are from the *IRAS* Point Source Catalog and Ladd et al. (1991a). The measurement at 2.7 mm is from observations using the Owens Valley Millimeter Array and was made with a beam of 5″ (Fuller et al. 1995, in preparation) and the measurements at 3.6 cm is from Anglada et al. (1995). Except for the emission at 3.6 cm, the emission at all these wavelengths is believed to arise from warm dust close to the young star. Integrating the observed fluxes from 3.6 cm to 1.25 μm, the upper limit to the total luminosity of the IRAS 18148−0440 is 14 $L_\odot$. The SED of IRAS 18148−0440 shows that most of the energy from this source is radiated at wavelengths between about 25 μm and 300 μm, similar to other heavily embedded young stars such as L1527 and B335 (Ladd et al. 1991a).

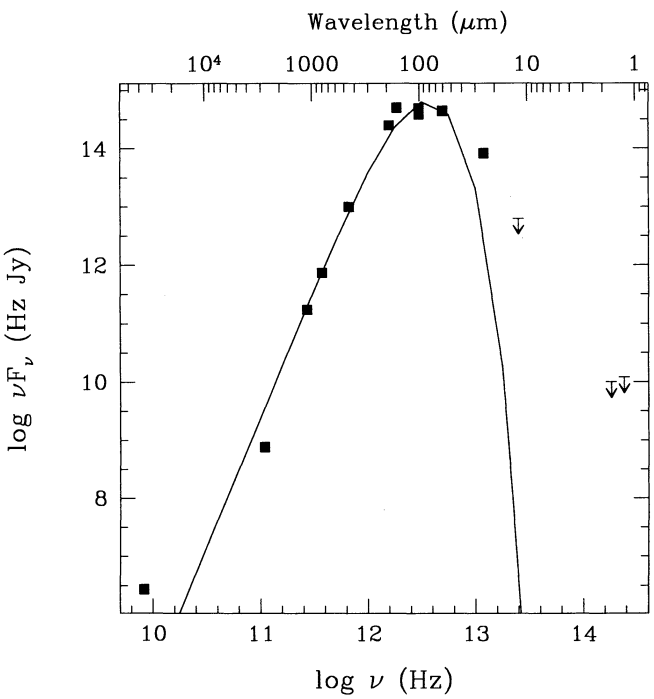

FIG. 4.—Spectral energy distribution of IRAS 18148−0440. The filled symbols show the measured fluxes from 3.6 cm to 25 μm. For all these points the uncertainties are smaller than the symbols shown. Upper limits at 12 μm (from *IRAS*) and J and H from this paper are also shown. The solid line shows the emission from 40 K dust which has an opacity profile which varies at $\nu^{1.5}$.

The SED of a young star can be characterized by the bolometric temperature, T_{bol} (Myers & Ladd 1993), which is directly correlated with the age of the star (Chen et al. 1995). T_{bol} is lowest for the youngest, most embedded stars and increases with stellar age until, for T Tauri stars, it is equal to the photospheric blackbody temperature. The SED of IRAS 18148−0440 gives $T_{bol} < 56$ K ($T_{bol} = 46$ K, if the upper limits in Fig. 4 are ignored). This is significantly less than the 97 K for the well-known young source L1551 IRS 5 and is comparable to the bolometric temperature of the youngest known source in Taurus, IRAS 04368+2557 (L1527) which has a bolometric temperature of 59 K (Chen et al. 1995). This low bolometric temperature of IRAS 18148−0440 suggests that it is a very young star, with an age of less than 4.2×10^3 yr. (with an uncertainty of a factor of 3).

Adopting a dust opacity, κ_ν, which varies as $\kappa_\nu \propto \nu^{1.5}$ (Pollack et al. 1994), the SED of IRAS 18148−0440 is reasonably well fitted by a single-temperature dust model with a temperature of 40 K (Fig. 4). Apart from underestimating the flux at 25 μm, the largest differences between the model and data are at the two longest wavelengths. However, the emission at 3.6 cm is believed to arise from the stellar wind and not from hot circumstellar dust (Anglada et al. 1995) and the 2.7 mm measurement was made with a significantly smaller beam than the JCMT observations between 1100 μm and 450 μm. Using a dust mass absorption coefficient of 5×10^{-3} g cm^{-2} (Pollack et al. 1994), the single-temperature fit shown in Figure 4 corresponds to a beam-averaged column density of 7×10^{22} H_2 cm^{-2} or an equivalent visual extinction of 78 mag assuming a conversion factor of 0.9×10^{21} between H_2 column density and visual extinction (Bohlin, Savage, & Drake 1978). Multiplying by the beam size, this gives a total mass of 0.35 $M_\odot$ of material within 1900 AU (9″.5) of the central young star.

4.2. *The Nebula and Outflow*

The shift in the location of the peak emission between J and K' is, at least in part, due to a gradient in extinction across the nebula. At the location of the peak of the J emission the nebula has J–K' and H–K' colors of ∼1.7 and ∼1.2 mag, respectively. However, at the peak of the K' nebula the J–K' color is ∼5.4 mag and the H–K' color is ∼4.1 mag. The J–2.22 μm and H–2.22 μm colors show the same reddening of the nebula close to the peak of the K' nebula, indicating the change in color is not due to changes in the molecular hydrogen line contribution to the K' flux. The reddening of the nebula near the *IRAS* source indicates that extinction is contributing to the wavelength-dependent shape of the nebula and that the extinction is larger near the young star.

At 2.2 μm the nebula around IRAS 18148−0440 is distinctly bipolar in shape. The eastern and western lobes of the nebula are spatially coincident with the red and blueshifted CO $J = 3 \rightarrow 2$ emission from the outflow, respectively (Fig. 3). The lower brightness of the eastern nebular lobe is consistent with its association with the receding, redshifted, outflow gas and it being observed through a larger column of dense gas than the approaching, western lobe. The geometry of the nebula and outflow suggests that the nebular emission is radiation from the central star scattered off the inner surface of the cavity excavated in the dense gas around the young star IRAS 18148−0440 by the star's wind.

If the near-infrared nebular emission is the result of scattering at the edges of the outflow cavity, the observed brightness profile results from a combination of the intrinsic brightness profile of the nebula plus the distribution of overlying extinction due to dust associated with the dense gas around IRAS 18148−0440. The weaker emission at J and H from the eastern lobe of the nebula is then consistent with the relatively higher dust opacities at these wavelengths than at 2.2 μm. The 2 μm images, where both lobes of the nebula are detected, provide an estimate of both the inclination angle of the outflow and the density profile within the dense gas around IRAS 18148−0440.

As can be seen from Figure 3, the eastern lobe of the nebula has a quite smooth brightness distribution which, overall, slowly declines at large angular distances from the central young star. This simple observation alone places a significant constraint on density profile within the dense gas. Since the nebula is scattered radiation from the central star, the nebula is intrinsically brighter close to the illuminating star. Therefore, in order to produce the relatively flat brightness distribution observed, there must be more extinction at small projected distances from the *IRAS* source. This conclusion is consistent with the redder color of the western lobe of the nebula close to the *IRAS* source, as discussed above.

A simple model for the brightness distribution of the nebula can be used to constrain both the angle between the axis of the outflow cleared cavity and the plane of the sky, α, and the density profile within the dense core surrounding IRAS 18148−0440. In this model IRAS 18148−0440 is assumed to be at the center of a spherical distribution of material which has a density profile which varies with distance r from the star as r^{-q}. The region cleared by the outflow is modeled as an evacuated cylindrical region of radius d extending along the outflow axis. The emission seen from the nebula is light directly from the central star which has been scattered to the observer by the walls of the cleared cavity. The model assumes that the scattered intensity is only a function of distance from the young star to the scattering location at the edge of the cleared cavity, of the scattering angle (assuming Rayleigh scattering), and the extinction due to the dense core material between the scattering location and the observer. The dense core size and density were fixed in the model to match the density and radius of the L483 NH_3 core (Fuller & Myers 1993).

Figure 5 shows the results for the ratio of the near nebular lobe intensity to the far nebular lobe intensity as a function of distance from the central star using this model. For this model the shape of this intensity ratio as a function of offset from the star depends on the density profile in the dense core, while the amplitude of the intensity ratio is a function of the inclination angle of the outflow axis to the line of sight. Models with density profiles $\propto r^{-q}$ with $q = 0$, 1, 2 are shown in Figure 5. Only models with $q > 1$ have sufficient extinction close to the young star to match the shape of the profile and the large intensity ratio observed close to the young star, in agreement with the argument presented above. The maximum observed intensity ratio indicates an inclination angle of ∼40°.

4.3. *The Density Structure Close to Young Stars*

Observations indicate that the density profile in dense cores varies with radius within a core as a power law with an exponent which varies from ∼ −1 in the outer regions to ∼ −2 in the thermally supported inner regions (e.g., Stüwe 1990; Yun & Clemens 1991; Fuller & Myers 1992). However, the behavior of the density profile in the very central regions of these cores is uncertain. Modeling of the SED of embedded young stars and the molecular-line emission from infalling envelopes around

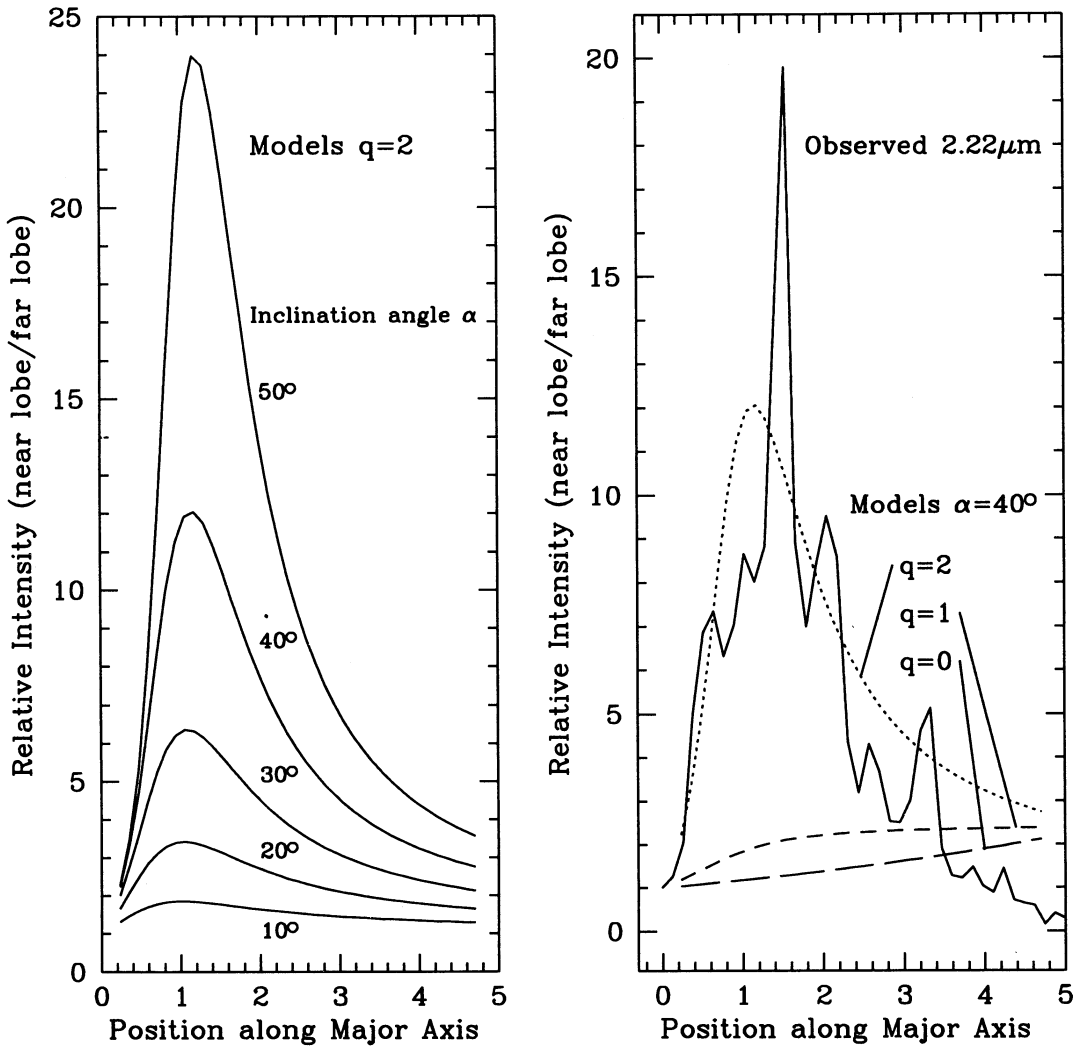

FIG. 5.—Model for the intensity ratio of the near nebular lobe to the far lobe as a function of distance from the central star for an outflow with cylindrical outflow lobes. The projected distance from the young star is measured in units of the cylinder radius, 2.6×10^{16} cm. The left panel shows the change in intensity ratio for different inclination angles for a number density profile $n \propto r^{-q}$ with $q = 2$. The right panel shows a slice along the major axis of the 2.22 μm image of IRAS 18148−0440 together with models with $\alpha = 40°$ and $q = 0$, 1, 2. The large intensity ratio close to the star is matched only by density profiles steeper than r^{-1}. The intensity ratio is reasonably fitted by a model where the outflow has an inclination of 40° to the plane of the sky and $q = 2$.

young stars indicate the presence of steep density profiles which vary with radius r as $r^{-1.5}$ to r^{-2} around the stars (Butner et al. 1991; Ladd et al. 1991b; Zhou et al. 1993), consistent with models for the structure and collapse of dense cores (Shu 1977; Terebey, Cassen, & Shu 1984). However, recent continuum observations of two young stars, L1551 NE and VLA 1623, have been interpreted as indicating much flatter density profiles around the stars (Barsony & Chandler 1993; André, Ward-Thompson, & Barsony 1993). The $r^{-0.5}$ density profiles claimed for these sources lead to the suggestion that the very youngest stars are surrounded by regions with relatively flat density profiles.

The SED of IRAS 18148−0440 suggests that it is in a similar evolutionary stage to the young sources L1551 NE and VLA 1623. Indeed, the bolometric temperature of IRAS 18148−0440, which is between 46 and 56 K, suggests that this source is somewhat younger than L1551 NE which has $T_{bol} =$ 75 K and is the second youngest source in Taurus. VLA 1623 is probably younger than either L1551 NE or IRAS 18148−0440 but its bolometric temperature is poorly determined as this source has not been detected at wavelengths shorter than 350 μm and so the peak of its SED is poorly defined.

Despite the apparently similar ages of these sources, the density profile in the circumstellar material around IRAS 18148−0440 is quite different from that claimed for L1551 NE and VLA 1623. The density profile in the material around IRAS 18148−0440 indicated by the analysis of the infrared nebula presented here, a profile steeper than r^{-1} and consistent with r^{-2}, is considerably steeper than the shallow $r^{-0.5}$ profiles claimed for the circumstellar regions of L1551 NE and VLA 1623. The implied density profile around IRAS 18148−0440 is consistent with both the extrapolation to smaller size scales of the density profiles seen at larger size scales in dense cores and the density profile expected from theoretical considerations.

4.4. *A Jet-Driven Outflow*

The outflow from IRAS 18148−0440 is highly collimated and the lobes of the outflow are nearly cylindrical in shape.

These are both features of young jet-driven outflows in regions with centrally condensed density profiles (Masson & Chernin 1993), suggesting that the IRAS 18148−0440 outflow is a young jet-driven outflow. There are two features of the molecular hydrogen emission from IRAS 18148−0440 which support this model for the source. First, the bow shock shape and its location at the end of the blueshifted CO lobe suggest that the bright H_2 emission knot traces the working surface at the end of the jet where the jet is impacting and sweeping up dense gas. More direct evidence for a jet from IRAS 18148−0440 comes from the narrow molecular hydrogen feature which is projected within the blueshifted CO outflow lobe. This jetlike feature extends from the peak of the blueshifted CO toward the emission knot at the far end of the lobe (Fig. 3) and appears to trace the path of the driving jet from the working surface back toward the central star. This H_2 emission associated with the jet may be due to shocks at the edge of the jet where material is being entrained in the jet. The molecular hydrogen emission in IRAS 18148−0440 therefore appears to show both types of jet entrainment discussed by De Young (1986), prompt entrainment at a working surface at the end of the jet and steady-state entrainment along the edges of the jet.

5. CONCLUSIONS

Both the infrared and submillimeter observations, and the CO outflow from IRAS 18148−0440 suggest that IRAS 18148−0440 is a very young source. The absence of a near-infrared counterpart of the central star and the far-infrared and submillimeter emission indicate that IRAS 18148−0440 has a large amount of circumstellar material with a column density within ~2000 AU of the central star corresponding to in excess of 70 mag of visual extinction. The bolometric temperature of IRAS 18148−0440 indicates an age of less than 4.2×10^3 yr, while the dynamical age of the CO outflow is $\sim 13 \times 10^3$ yr. The apparent discrepancy in the implied age of IRAS 18148−0440 is probably not significant given the uncertainties and approximations involved in making the ages estimates. For example, Chen et al. (1995) estimates a factor of 3 uncertainty in the ages of sources derived from a source's bolometric temperature.

At J, H, and K' there is extended nebulosity associated with IRAS 18148−0440. The spatial variation in the color of this nebular emission and its brightness distribution constrain the density in the material around the young star to vary with radius more steeply than r^{-1}.

The brighter lobe of the extended near-infrared nebula associated with IRAS 18148−0440 is spatially coincident with the blueshifted lobe of the CO outflow from the source. This spatial coincidence suggests that the nebular emission is radiation scattered from the wall of the cavity cleared by the stellar wind. Projected on to the blueshifted CO lobe there is a jetlike region of H_2 emission which terminates in a bright knot of H_2 emission located at the end of the CO lobe. The knot of emission appears to be the working surface where the jet from the central star is impacting the dense gas surrounding the young star. Together with the highly collimated nature of the outflow and the cylindrical shape of the lobes of the infrared nebula, this morphology of the H_2 emission suggests that the IRAS 18148−0440 outflow is an example of a young, jet driven outflow.

With its large amount of circumstellar material and well collimated outflow and centimeter radio continuum emission, IRAS 18148−0440 appears to be at a very early stage in its evolution. It is similar in its properties to a small number of other low luminosity embedded stars, such as VLA 1623 and L1527, the so called Class 0 sources (André et al. 1993). Like these sources, its youth makes IRAS 18148−0440 a good candidate for detecting the circumstellar material which is undergoing gravitational collapse to form the central young star.

G. A. F. would like to thank Luis Rodriguez for communicating the results of Anglada et al. to us before publication. G. A. F. acknowledges the support of a NRAO Jansky Fellowship. G. A. F. thanks the Laboratory for Millimeter Wave Astronomy at the University of Maryland for their hospitality while writing parts of this paper. E. A. L. acknowledges support for this work from NSF grant No AST 93-14847 to the University of Maryland and from NASA through Hubble Fellowship grant HF-1047.0193A awarded by the Space Telescope Science Institute, which is operated by the Association of Universities for Research in Astronomy, Inc., for NASA under contract NAS 5-26555. Kitt Peak National Observatory is operated by the National Optical Astronomy Observatory under contract to the National Science Foundation.

REFERENCES

André, P., Ward-Thompson, D., & Barsony, M. 1993, ApJ, 406, 122
Anglada, G., et al. 1995, in preparation
Aspin, C., McCaughrean, M. J., Casali, M. M., & Geballe, T. R. 1991, A&A, 252, 299
Bally, J. R., Lada, E. A., & Lane, A. P. 1993, ApJ, 418, 322
Barsony, M., & Chandler, C. J. 1993, ApJ, 406, L71
Bohlin, R. C., Savage, B. D., & Drake, J. F. 1978, ApJ, 224, 132
Butner, H. M., Evans, N. J., Lester, D. F., Levreault, R. M., & Strom, S. E. 1991, ApJ, 376, 636
Chen, H., Myers, P. C., Ladd, E. F., & Wood, D. O. S. 1995, ApJ, 445, 377
De Young, D. S. 1986, ApJ, 307, 62
Fuller, G. A., & Myers, P. C. 1992, ApJ, 384, 523
———. 1993, ApJ, 418, 273
Hodapp, K. W., Capps, R., Strom, S. E., Salas, L., & Grasdalen, G. L. 1988, ApJ, 335, 814
Hubble, E. 1922, ApJ, 56, 400
Jensen, E. L. N., Mathieu, R. D., & Fuller, G. A. 1995, ApJ, submitted
Kenyon, S. J., Calvet, N., & Hartmann, L. 1993, ApJ, 414, 676
Kenyon, S. J., Whitney, B. A., Gomez, M., & Hartmann, L. 1993b, ApJ, 414, 773
Ladd, E. F., Adams, F. C., Casey, S., Davidson, J. A., Fuller, G. A., Harper, D. A., Myers, P. C., & Padman, R. 1991a, ApJ, 366, 203
Ladd, E. F., et al. 1991b, ApJ, 382, 555
Masson, C. R., & Chernin, L. 1993, ApJ, 414, 230
Myers, P. C., & Ladd, E. F. 1993, ApJ, 413, L47
Parker, N. D. 1988, MNRAS, 235, 139
———. 1991, MNRAS, 251, 63
Parker, N. D., Padman, R., & Scott, P. F. 1991, MNRAS, 252, 442
Pollack, J. B., Hollenbach, D., Beckwith, S., Simonelli, D. P., Roush, T., & Fong, W. 1994, ApJ, 421, 615
Scoville, N. Z., Hall, D. N. B., Kleinmann, S. G., & Ridgeway, S. T. 1982, ApJ, 253, 136
Shu, F. H. 1977, ApJ, 214, 488
Stüwe, J. A. 1990, A&A, 237, 178
Tamura, M., & Yamashita, T. 1992, ApJ, 391, 710
Tamura, M., Gatley, I., Waller, W., & Werner, M. W. 1991, ApJ, 347, L25
Terebey, S., Cassen, P., & Shu, F. H. 1984, ApJ, 286, 529
Wilking, B. A., Claussen, M. J., Benson, P. J., Myers, P. C., Terebey, S., & Wootten, A. 1994, ApJ, 431, L119
Yun, J. L., & Clemens, D. P. 1991, ApJ, 381, 474
Zhou, S., Evans, N. J., Koempe, C., & Walmsley, C. M. 1993, ApJ, 404, 232